



R&D on Microstrip IR Transparent Silicon Sensors*

M. Fernández, J. González, S. Heinemeyer, R. Jaramillo,

A. López, C. Martínez, A. Ruiz, I. Vila

Instituto de Física de Cantabria, Universidad de Cantabria and CSIC, Santander (Spain)

M. Lozano, G. Pellegrini, E. Cabruja

Centro Nacional de Microelectrónica, IMB-CNM/CSIC, Barcelona, (Spain)

December 3, 2007

Abstract

The next generation of tracking systems, as the one envisaged for the International Linear Collider (ILC) will demand track momentum resolutions one order of magnitude better than current state-of-the-art trackers. Mechanical stabilities coping with the precision of such measurements should either be provided by the construction of the supporting structure (currently out of the technological reach) or monitored using an alignment system. Based on the successful experience of AMS and CMS tracker systems, we propose to use infrared laser beams traversing consecutive layers of silicon detectors to align them with respect to the beams. Laser beam “pseudo-tracks” work like infinite momentum particle tracks. Yet we have slightly altered the thicknesses of the different material layers and the pitch/strip-width ratio of the sensors to obtain maximum transmittance to the IR beam, without modifying its performance as a tracking device. Replacement of the Aluminum electrodes by semitransparent oxides like ITO have also been considered. Transmittances close to 80% for IR beams can thus be obtained.

*This work has been carried-out within the SiLC (Silicon for the Linear Collider) collaboration, a generic R&D collaboration to develop the next generation of large area Silicon Detectors for the ILC. It applies to all detector concepts and gathers teams from all proto-collaborations. The collaborators of SiLC which are also EUDET partners are forming the SiTRA (Silicon Tracking) group.

1 Introduction

High precision measurements demand tightly controlled environments. Metrology laboratories calibrating optomechanical systems can provide long term mechanical stabilities of order $1\ \mu\text{m}$ by controlling environmental conditions and by using precision mechanics. Translation of these conditions to a high energy physics environment is something very hard to realize. In real experiments, environmental disturbances like local temperature gradients (produced by operation and cooling of detectors) or humidity changes affect the stability of any supporting structure at the micrometer level. Compacity of current detector designs and the need for minimum multiple scattering contribution from any extra added material push forward the idea of integrated alignment systems.

For the particular case of tracking detectors, a very elegant alignment method has been recently proposed and implemented [1] at the Alpha Magnetic Spectrometer (AMS) [2] and subsequently adopted [3] by the tracking system of the Compact Muon Solenoid [4]. In a nutshell, consecutive layers of silicon sensors are traversed by IR laser beams which play the role of infinite momentum tracks (not bent by the magnetic field). Then, the same sophisticated alignment algorithms as employed for track alignment with real particles can be applied to achieve relative alignment between modules to better than few microns. Furthermore, since IR light produces a measurable signal in the silicon bulk, there is no need for any extra readout electronics. And all these advantages come to a minimum cost: the aluminum metalization (backelectrode) of the sensor needs to be swept away in a circular window with a diameter of few millimeters to allow the IR beam to pass through.

We will start by reviewing the performance of microstrip silicon sensors in the alignment system of the AMS and CMS experiments. Then we will present an optical simulation of the transmission of light inside a typical microstrip detector. The departing point will be an idealized version of the sensor and then we will move towards a real sensor case. Finally an optimization of the current design will be presented.

2 Review of former IR-transparent silicon alignment systems

2.1 AMS Tracker Alignment System

The precursor flight of the AMS experiment showed that optically generated straight tracks could be used to follow up changes of the geometry with a position accuracy better than $2\ \mu\text{m}$ [5].

For AMS-02, silicon detectors have been made of high resistivity ($\geq 6\ \text{k}\Omega\ \text{cm}$) n-doped $300\ \mu\text{m}$ thick Si wafers covered with longitudinal heavily p⁺-doped Si strips on one side (p-side) and with transversal n⁺ strips on the other. The implantation (readout) strip pitch is $27.5\ (110)\ \mu\text{m}$ for the p-side and $104\ (208)\ \mu\text{m}$ for the n-side. The strips are AC-coupled to the readout chips. The alignment system is equipped with 2×10 pairs of beams at $\lambda = 1082\text{nm}$ crossing selected sensors out of the 8 Si planes. For these selected

sensors the aluminum backelectrode has been locally removed in 4 windows (2 in AMS-I sensors, see Fig. 1.a) and the thicknesses of the Si₃N₄ and SiO₂ layers on both sides of the detector have been properly tuned to act as an Anti-Reflection Coating (ARC). In addition, and only on the alignment areas, the readout strip metalization has been narrowed to 10 μm width and removed at the implants not used for readout (Fig. 1.b). The transmittance of the sensors after all these optimizations is above 50% (see Fig. 1.c).

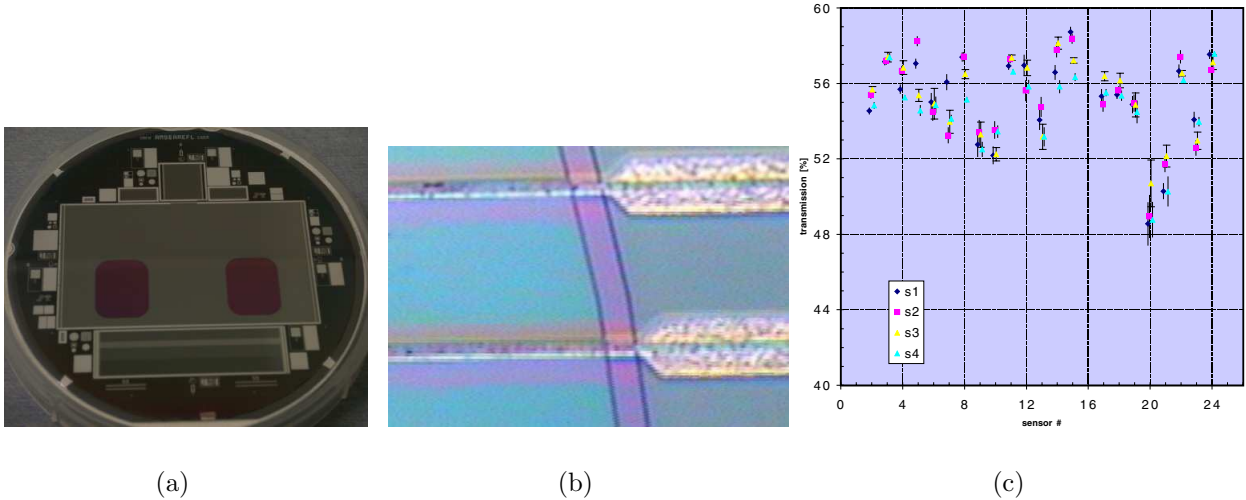


Figure 1: a) View of the 2 alignment passages of an AMS-I silicon sensor. b) Zoom of the sensor backside, clearly showing the strip narrowing of the readout strips at the transition between coated/uncoated areas. c) Transmittance distribution for a whole sensor batch ([6]).

2.2 CMS Tracker Alignment System

Sensors of different thicknesses and lengths were produced for CMS [7]. Thin and short (thick and long) sensors 320 (500) μm thick, having a substrate resistivity in the range 1.5-3.5 (4-8) $\text{k}\Omega\text{cm}$ were produced by Hamamatsu [8] (STM [9]). A uniformly metalized n^+ layer implanted on the backside provides an ohmic contact between the bulk and metal layer keeping the leakage current low. p^+ implantation was used on the front side to define strip-shaped diodes made of multiple layers of dielectrics covered by metal Al strip electrodes. The width of the implanted strip is a quarter of the pitch to keep the strip capacitance constant. The Al metal overhangs by 15% on each side of the implant. The pitch varies between 80-205 μm , depending on the radial position of the sensor. Sensors are AC coupled to readout strips.

A subset of Si sensors was specially treated for alignment. They have been double polished¹ by the vendor and backside coated by MSO Jena [10] with an ARC made of 95

¹Standard sensors are polished on the front and acid etched on the back.

nm Ta₂O₅ on 94 nm SiO₂. The Al metalization has been removed in a circular window of 10 mm diameter. In total 640 sensors have been coated and specially treated for alignment [11].

The system employs a total of 40 (+20 spares) laser diodes working at $\lambda=1075\pm 3.5$ nm having a spectral width $\Delta\lambda=2.4\pm 0.9$ nm. For ease of comparison, measurements of the sensors at the AMS working wavelength showed a transmission (reflection) of 21% (6%). The lower optical performance, as compared with AMS, comes from the fact that only one of the sides of the detector could be coated and also because the readout strips were not narrowed.

In order to reach the furthestmost 5th Si plane, the beam intensity is increased such that some of the 4 detectors downstream can be saturated while not being measured. This system has been proved to measure the overall deformations and movements of the supporting structure with a precision better than the 100 μ m needed for the online track reconstruction algorithms [4].

3 SiLC hybrid alignment baseline

Precise alignment and positioning are crucial in order to achieve the very high spatial resolution performance required for the tracking detectors in the ILC environment. Adding the smallest possible material budget in the overall tracking system is another crucial issue. The IR alignment system (also called hybrid alignment system) proposed within the SiLC collaboration strictly fulfills this constraint.

Last section has stressed the importance for integrated tracker alignment systems of having a sensor providing maximum transmittance with moderate absorption in the IR range. Our goal in this paper is first to identify what are the factors limiting the clean propagation of an IR beam through a typical silicon microstrip detector. Once the propagation inside the detector is understood, we will introduce the needed changes to the design to achieve maximum transmission. The higher the transmission value, the more detectors can be aligned with the same beam. The set of modifications should be of general applicability and do not restrict only to the particular ILC design.

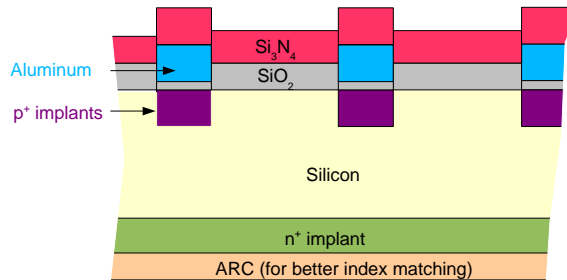


Figure 2: *Section of a representative silicon microstrip sensor employed for a realistic simulation of the beam propagation (drawing not to scale).*

This project is a collaborative effort between the Physics Institute from Cantabria (IFCA) and the Spanish National Centre for Microelectronics at Barcelona (CNM) where the prototypes of the simulated detectors will be produced. Our starting point for this work is the kind of sensor depicted in Fig. 2 which will be referred from here onwards as CNM sensor. This is currently a working sensor produced at CNM. For the time being, it is important to stress the difference between the upper and lower half of the detector. While the bottom half is made out of smooth planoparallel slabs of material, the upper materials are fractured and follow the underlying strip segmentation. This periodicity will induce diffraction of the incoming wave which will be propagated through this and the nextcoming sensors. It is our intention to study and simulate the contribution of the diffraction to the overall sensor transmission.

We have assumed periodicity of the electrodes of $p = 50 \mu\text{m}$ (this is the SiLC baseline). The layer below the strips is a combination of Silicon implants (p^+ doped Si) of the same width as the strips and approximately $1.1 \mu\text{m}$ thick. Above the strips, there is a layer of SiO_2 ($\sim 1 \mu\text{m}$ thick). The sensor is protected with a passivation layer of Si_3N_4 ($\sim 1.5 \mu\text{m}$ thickness). Below the implant line, we have a silicon bulk of $285 \mu\text{m}$ thickness, and the ohmic contact made of n^+ doped silicon $\sim 1.1 \mu\text{m}$ thick. A proper choice for the thickness of the upper layers should work as an ARC coating (although the relative order of the layers is not the optimal in terms of refraction index). On the bottom half of the detector, an ARC made of Si_3N_4 and SiO_2 ensures a smooth Si-to-air refraction index transition. In case we can use transparent electrodes (see next section) there will be an extra layer at the bottom of this design. If the electrodes are made of Al, instead, a circular window in the Al must be opened to let light propagate through (not shown in the drawing).

4 Simulation of ideal Silicon Microstrip detectors

The simulation of the microstrip Si sensors will be accomplished in 2 steps. First we will simulate the sensor shown in Fig. 2 considering it as a stack of perfect homogeneous layers and will calculate its optical functions: transmittance $\%T$, absorptance $\%A$ and reflectance $\%R$. Then we will take into account the segmentation of the strips and will calculate the same figures. Finally we will optimize the sensor layout for maximum transmittance.

4.1 Optical properties of the materials

Any homogeneous isotropic optical medium is solely characterized by its complex refraction index: $N = n - ik$, where k is the so-called optical extinction coefficient. The refraction index changes with the wavelength $N = N(\lambda)$. Sources of tabulated refraction indexes exist over a wide range of wavelengths. For this work we have used the following ones:

- $\text{SiO}_2, \text{Si}_3\text{N}_4, \text{Al}$, from reference [12]

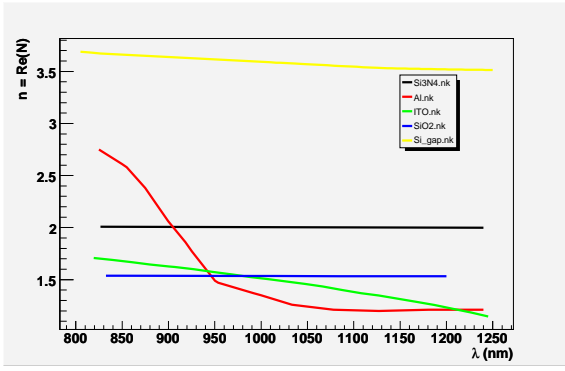


Figure 3: *Real part of the refractive index of the materials used for the simulation*

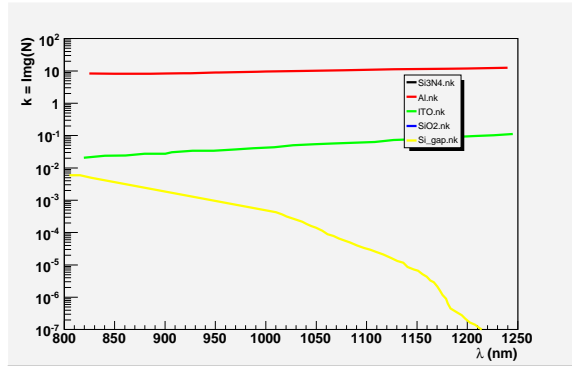


Figure 4: *Extinction coefficient (logarithmic scale) of the various materials employed in the simulation. SiO_2 , Si_3N_4 are non absorbing*

- Precision measurements of Silicon within the absorption gap [13]
- Doped (n,p) silicon [14]

A comparison of the real part of the refractive index n , around the wavelength range of interest, for the different materials is shown in Fig. 3. For materials without absorption ($k = 0$), n determines the amount of reflected and transmitted energy. For instance, two layers with very different refractive indexes will have higher reflectance than 2 layers with similar refractive indexes. In this sense, optical designs pursuing high transmittance should avoid stacking together layers with very different refractive indexes. Transitions between different layers should be smooth and monotonous in terms of refractive index. Since Si is the highest index material, *coatings* like $\text{Si} \rightarrow \text{Si}_3\text{N}_4 \rightarrow \text{SiO}_2$ will perform better than $\text{Si} \rightarrow \text{SiO}_2 \rightarrow \text{Si}_3\text{N}_4$.

Figure 4 compares the different layers in terms of the extinction coefficient. The intensity of the incident radiation is attenuated to $1/e$ of its initial value after a distance given by

$$\frac{1}{\alpha} = \frac{\lambda}{4\pi k} \quad (1)$$

α is the so-called absorption coefficient and has the units of inverse distance. Materials with a numerically high extinction coefficient k are less transparent than those with lower values. For instance, $1 \mu\text{m}$ thickness of Al attenuates the equivalent of $10^5 \mu\text{m}$ of Si at $\lambda = 1 \mu\text{m}$.

4.2 Optical properties of Si

The absorption in the Silicon layer will determine the amount of signal deposited in the silicon bulk by the IR beam. A very low absorption would avoid reconstruction of the laser beam centroid. On the other hand, too high absorption will saturate the dynamical range of the ADC and will avoid high transmittance to the sensors downstream.

Si is well known to be almost transparent at IR wavelengths. From Fig. 4 $k(\lambda = 1100nm) \sim 0.3 \times 10^{-4}$, so the penetration depth is almost $1/\alpha = 3000 \mu m$. Fig. 5 shows the absorption for a slab of Si $320 \mu m$ thick in the near infrared (NIR) region. Depending on the actual thickness and wavelength chosen, absorption values ranging 1-10% are possible. Considering that typical laser diodes can produce more than 10^8 photons per pulse and assuming 1 MIP in Si produces $\sim 25000 e^-$ in $280 \mu m$ of Si, laser signals will range between 40-2000 MIPs.

4.3 Optical properties of doped Si

Doped (both n or p) silicon optical properties are very different from intrinsic silicon. Same way as the impurities vary the electrical conductivity of Si by several orders of magnitude, so does the optical extinction coefficient k upon doping. Figure 6 shows how the absorption coefficient changes as a function of the wavelength for various doping concentration levels (p-doping) [14]. This figure is very similar for n-doping. A very compact parametrization of these curves can be found in reference [15].

4.4 Interference by multiple reflections

When light impinges at the interface between 2 homogeneous media, the energy is split between reflected and transmitted waves. If the final medium is lossy (characterized by a complex refraction index), part of the energy transmitted will be absorbed. If this medium has a finite thickness, then some light will be reflected back at the last boundary. Both direct transmitted and reflected beams will interfere many time and the resulting intensity distribution, provided that the thickness is not sensibly bigger than the wavelength, will show typical interferential maxima and minima. By calculating Fresnel coefficients at each interface (see for instance [16]), one can compute the amount of energy reflected, transmitted and absorbed by the film.

When scaling up this argument for an arbitrary number of layers, one needs to consider contributions from all layers of the stack. A number of different formulisms allow the calculation of the resulting optical functions. For two different solutions to the multiple reflections problem, see for instance references [17] (matrix method) and [16], [18] (Fresnel coefficients). In this work, we have followed Fresnel method.

Fig. 7 shows a cross section of an idealized detector. Each layer is assumed to be infinite in Y direction (we therefore neglect reflections coming from the sensor vertical walls), homogeneous and perfectly planoparallel. From top to bottom we have:

- a layer of silicon nitride (Si_3N_4) which acts as a passivation layer.

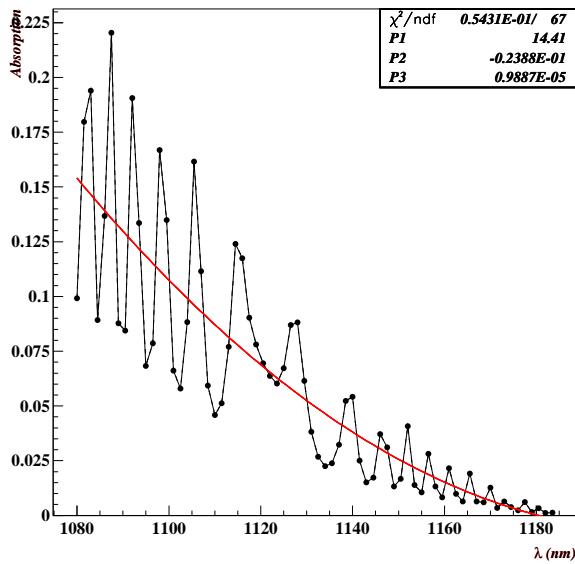


Figure 5: *Absorption for a slab of 320 μm Silicon, with a polynomial fit overimposed.*

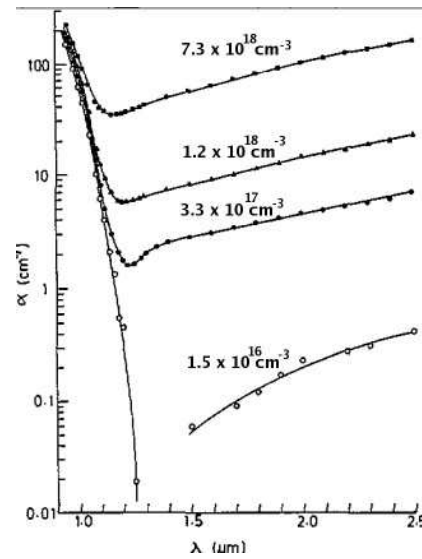


Figure 6: *Absorption coefficient for Si at various doped levels, from [15]. Free carrier absorption begins to dominate at wavelengths above 1100 nm, roughly.*

- Since we do not know yet how to simulate non homogeneous media (see section 5 for that), we cannot use neither aluminum strips nor strip implants below them. For the ideal simulation, substitution of Al strips by a continuous layer of Al would not work either since the Al layer, being a perfect reflector, would prevent light from being transmitted. Therefore we can try to substitute Al by a Transparent Conductive Oxide [19] such as Indium Tin Oxide (ITO) or Aluminum-doped Zinc Oxide (AZO). These materials are transparent to light for thickness of layers of order 100 nm.
- Silicon Oxide (SiO_2).
- Silicon bulk. Strip implants above the bulk (and below the strips) are modeled by a continuous layer of p^+ doped Silicon. The continuous n^+ layer below is well described by another continuous layer.
- Anti-reflection coating (ARC): any material(s) with a refraction index in between that of Si and air can be used to soften this index gap. We have chosen Si_3N_4 and SiO_2 .
- A transparent backelectrode made of ITO

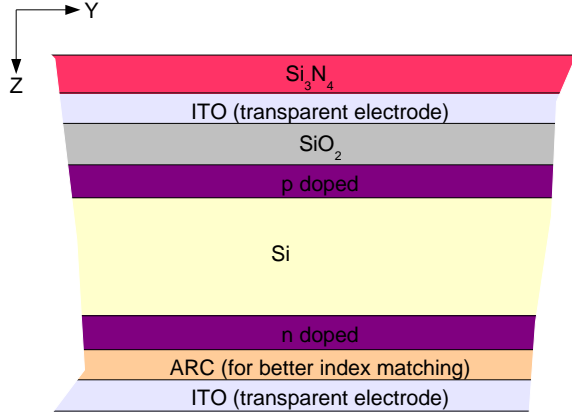


Figure 7: *Sketch of an ideal microstrip silicon sensor (infinite extension perfect planoparallel layers, no strips). Drawing not scaled.*

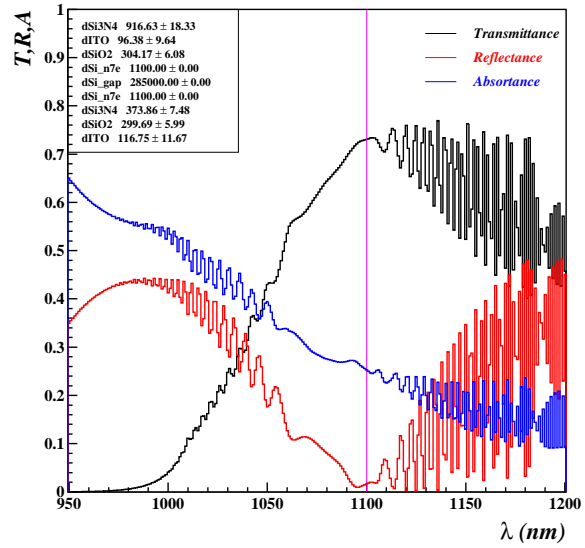


Figure 8: *Optical functions for an idealized sensor as the one shown in the left. The box shows the actual layer order and thicknesses.*

The simulation of such an ideal sensor using multiple reflections is shown in Fig. 8. The three optical functions are displayed as a function of the wavelength. The actual layers and their thicknesses are summarized in the inlaid box. For completeness, we also show in Fig. 9 the transmittance of each of these layers individually. The thickness of the materials from Fig. 8 have been optimized to achieve maximum transmittance at 1100 nm (the vertical pink line shows the optimization wavelength). The shape of the transmittance curve (blue line) shows a strong absorption up to 1000 nm due to both the extinction coefficient of Si and its thickness. Indeed, although the extinction coefficient of ITO is higher than that of Si (see Fig. 4) the limiting factor here is the thickness of the latter (285 μm versus 0.1 μm for ITO). The quick oscillations for $\lambda > 1100$ nm are due to the thickness of the Silicon slab, (see central plot in Fig. 9). Even though the rest of materials (SiO_2 , Si_3N_4 , ITO, ...) do not leave their stamp in the overall transmittance picture, they make multiple reflections possible, and therefore, allow optimization of the design at the working wavelength. In particular, we observe the negligible reflectance value (red line) obtained from the maximization of the transmittance with minimization of the reflectance.

Finally, the blue line describes the absorption of the whole stack, again, mainly induced by the combination of Si extinction and Si thickness.

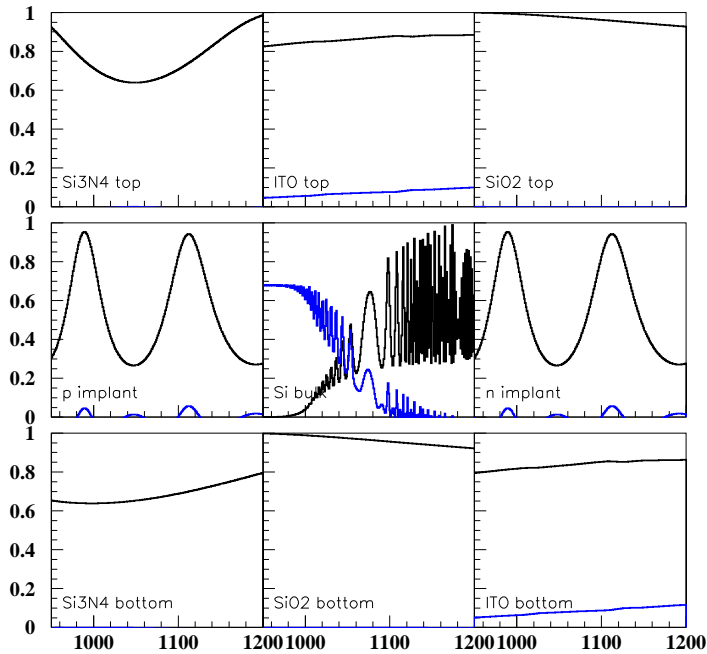


Figure 9: *Transmittance (black) and absorption (blue) for all the layers of the sensor stack, with thicknesses as given in Fig. 8.*

5 Full optical simulation of Silicon Microstrip detectors

In a real sensor as that depicted in Fig. 10, there are several layers of “diffraction gratings” overlaid. In general, the beam will be diffracted when the incoming wave faces areas of size comparable to the wavelength, and different refractive index. Due to the segmentation of the strip electrodes, all layers above them will be forced to adapt to the underlying topography.

A discontinuous layer, will act as a linear grating, reflecting and transmitting light in a discrete set of directions. When the diffracting obstacle is perfectly black, that is, all radiation falling on it is absorbed and none reflected, the standard scalar theories for diffraction of Young, Fresnel or Kirchoff can be applied [16]. This approach fails to reproduce the actual energy partition when the grid material is not perfectly opaque. In our real case scenario neither ITO, nor Al gratings are opaque. They transmit or reflect light. Besides, SiO_2 and Si_3N_4 layers above the electrodes are another example of transparent grating obstacles. Under such conditions, a rigorous solution of Maxwell equations is needed. Their rigorous nature [20] can be found in the strict solution of the electromagnetic-boundary-value problem: a solution has to be found that strictly satisfies Maxwell’s equations in the input, grating and output region and that fulfills the

boundary conditions for the tangential electric and magnetic field components at the respective interfaces.

In this work, two different rigorous methods have been employed to simulate the real sensor. The RCWA (Rigorous Coupled Wave Analysis) [20], [21] and the Eigenmode Expansion [22], [23] (also known as Modal Method). Their difference resides in their alternative representation of the e.m. field in the binary grating region. The eigenmode method chooses to represent the field inside the grating as a weighted sum of independent eigenmodes, each satisfying Maxwell's equations. These exact eigenfunctions of the grating are similar to modes in a waveguide. The boundary conditions can be fulfilled for a weighted summation over all the modes; the individual modes, however, do not fulfill these conditions. The RCWA on the contrary expands the field inside the grating in terms of plane waves. The total field is a weighted sum of inhomogeneous coupled plane waves. The individual plane waves are phase matched to the respective diffracted waves of the Rayleigh expansion of the field outside the grating. The individual plane waves do not satisfy Maxwell's equations. The waves are not independent and couple back and forth between each other. The propagating directions of these plane waves are given by a grating equation of the form (see Fig. 10):

$$\sin \theta_m = \sin \theta + m \frac{\lambda}{d} \quad (2)$$

where θ is the incident angle, θ_m the diffraction angle, λ the wavelength in air, m an integer representing the order of diffraction (m can be negative too) and d the pitch. Note that still under normal incidence ($\theta = 0$), there will be modes diffracted at $\theta \neq 0$.

5.1 Rigorous diffraction solvers: software

Due to the complexity of both the physical problem and the mathematics involved in solving it, we spent some time searching for programs that might have already tackled this problem. Fortunately, we found two opensource projects from the photonics group of the Department of Information Technology at Ghent University (Belgium). The first one, RODIS [24] solves Maxwell equations implementing the RCWA method. It is specially suited for linear gratings. This program is not under development anymore, but the current version efficiently solves 1D and 2D diffraction problems. The second one, CAMFR [25] implements an Eigenmode Expansion solution of the Maxwell equations. It is particularly flexible and can address problems with intricate geometries. Besides that, it accepts different excitation fields and provides a display of the e.m. field and its intensity on the diffraction grating. This program is supported by developers. Both programs are written in C++ but provide a convenient Python interface [26]. We have used in both cases the linux versions.

Since these methods solve exactly Maxwell equations, they are also applicable for the cases of ideal sensor conditions. Indeed we have crosschecked that both rigorous methods reproduce the same results as obtained with Fresnel coefficients.

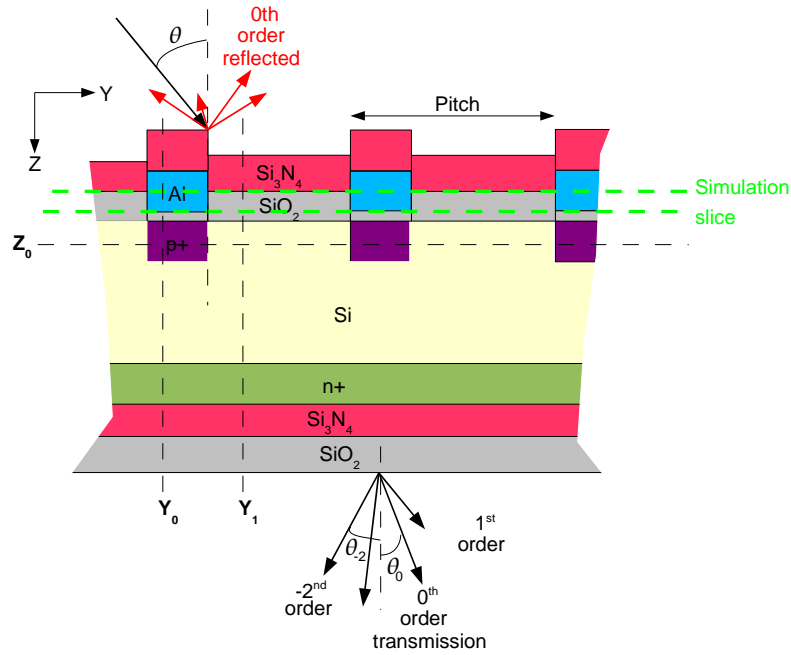


Figure 10: *Incoming energy splits in a set of reflection and transmission directions. Represented only until $\pm 2^{\text{nd}}$ order. Shown as well the reference frame, and a typical slice as used in the simulation.*

6 Simulation of a realistic sensor

Employing the terminology introduced in section 5, we will maximize the amount of energy going into the transmitted 0^{th} order (see eq. 2) while minimizing the amount of energy reflected into the 0^{th} reflected order. In other words, we will try to lose as less energy as possible at maxima other than the central transmitted maximum. As mentioned by [11], it is much easier to fit the central maximum when a laser beam is utilized for the real measurements.

To simulate a real sensor as that from Fig. 10, we slice the layers horizontally (in the plane of the grating along Y , see Fig. 10) with the constraint that *in each slice* only one refraction index can be present for any fixed Y_0 , although the refraction index at Y_0 can be different from that at Y_1 . This is equivalent to say that the wave propagates in this slice with a constant $n(z_0, y); \forall y$.

We have worked with the CNM layout for the microstrip silicon sensor (see section 3). The same calculations as those shown here for this configuration will be reproduced for the CMS sensor [27]. Nominal parameters for the strip layer are pitch= $50 \mu\text{m}$ and strip width= $12.5 \mu\text{m}$. These parameters are subject to further optimization.

The first step we can do is to simulate the same structure as that of Fig. 8 using ITO as electrode material in the strips. The result can be seen in Fig 11. As one can see, the difference between this simulation including the strips with respect to the same simulation including continuous layers of electrodes is significant. Not only the overall

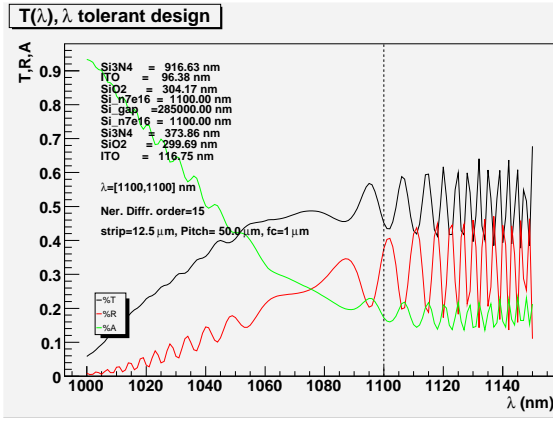


Figure 11: *Realistic simulation of the same Si microstrip detector as shown in Fig. 8. This simulation includes diffraction at the strips.*

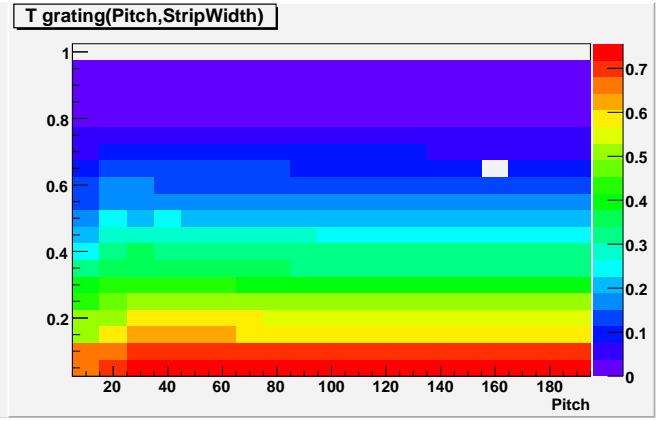


Figure 12: *Transmittance as a function of the grating pitch (horizontal) and strip width (vertical), calculated for at $\lambda = 1100$ nm.*

transmittance is lower, but also the position of the maxima are different.

To improve this picture (besides changing the thicknesses of the materials), one can try to study first the dependence of the transmission as a function of the grating parameters, namely pitch and strip width. After finding a proper value for these 2 parameters, we can try to maximize the transmittance by changing the thicknesses of the layers.

Figure 12 shows the transmittance of a sensor for different pitch (horizontal axis) and strip width conditions (vertical axis). The thicknesses of the material layers are summarized in table 1, although similar trends can be obtained departing from another set of thicknesses. In this figure, the strip width is defined as a fraction of the pitch ($50 \mu\text{m}$). Note that this design contains Aluminum as the material in the electrodes. This is the reason why, the transmittance drops to zero when the strip with is numerically equal to the pitch. In this case, the layer of Al becomes continuous and therefore no light can be transmitted. From Fig. 12 it is clear that the transmittance depends mostly on the strip width. Indeed, the narrower the strips are (in the Y coordinate), the more intensity can go through the layer with electrodes. From this figure we chose a pitch= $50 \mu\text{m}$ (SiLC nominal value) and a strip width of 10% the pitch. A transmittance value $T \sim 0.7$ should be achieved. Note that the transmittance grows almost linearly on the strip width. We recall that the change of the pitch/strip-width is only needed in the alignment window and not in all the sensor.

Once optimum grating parameters are selected, we can try to study the effect of varying the thickness around a stable configuration. This can give us an idea of which are the parameters the transmittance depends most. This is also important to calculate the

Material	Thickness (nm)
Si ₃ N ₄	2304
Al	916.2
SiO ₂	1502.5
Si, p ⁺ doped	1100
Si bulk	285×10 ³
Si, n ⁺ doped	1100
Si ₃ N ₄	989.6
SiO ₂	176.5

Table 1: *Nominal thickness of the material layers of the CNM microstrip detector employed for the (pitch,width) scan.*

tolerances of the design. Figure 13 contains left to right, top to bottom, plots of the transmittance of the reference sensor design where only one of the material thicknesses are changed (vertical coordinate). The scan is done as a function of the wavelength (horizontal axis). The rest of layer thicknesses are those shown in table 1. The pitch is 50 μm and the strip width is 5 μm , as learned from Fig. 12.

Using the analysis shown in Fig. 13 we can select a wavelength for which the parametrized transmittance has a relative maximum. We have chosen $\lambda = 1100$ nm. Once the wavelength is fixed, we can select the thickness value for each layer that yields maximum transmittance. Except for the case where the material might have a very high absorption, the transmittance will display a periodicity with thickness. Choosing any of those values will not provide an absolute extreme, but will yield a good starting point for our optimization and allows to spot regions of one parameter that should be avoided. Finding an absolute extreme within a range of parameters, requires all the thicknesses to be changed simultaneously. We can build a χ^2 minimization function defined as:

$$\chi^2 = \sum_{\lambda=1100\pm\Delta\lambda} \sum_{d_i} (T(\vec{d}_i, \lambda) - T_{max})^2 + R(\vec{d}_i, \lambda) \quad (3)$$

where \vec{d} is a vector with the thicknesses of the different materials, T_{max} a reference value we want to achieve. The sum in λ should cover the spectral width of the laser ($\Delta\lambda$). The χ^2 function will be minimum for a set thickness that fulfill $T \sim T_{max}$ and $R \sim 0$.

Applying eq. (3) for $\lambda = 1110$ nm and $\Delta\lambda = 0$ we achieve an optimized design as that shown in Fig. 15. The difference with respect to Fig. 14 is small in terms of absolute %T.

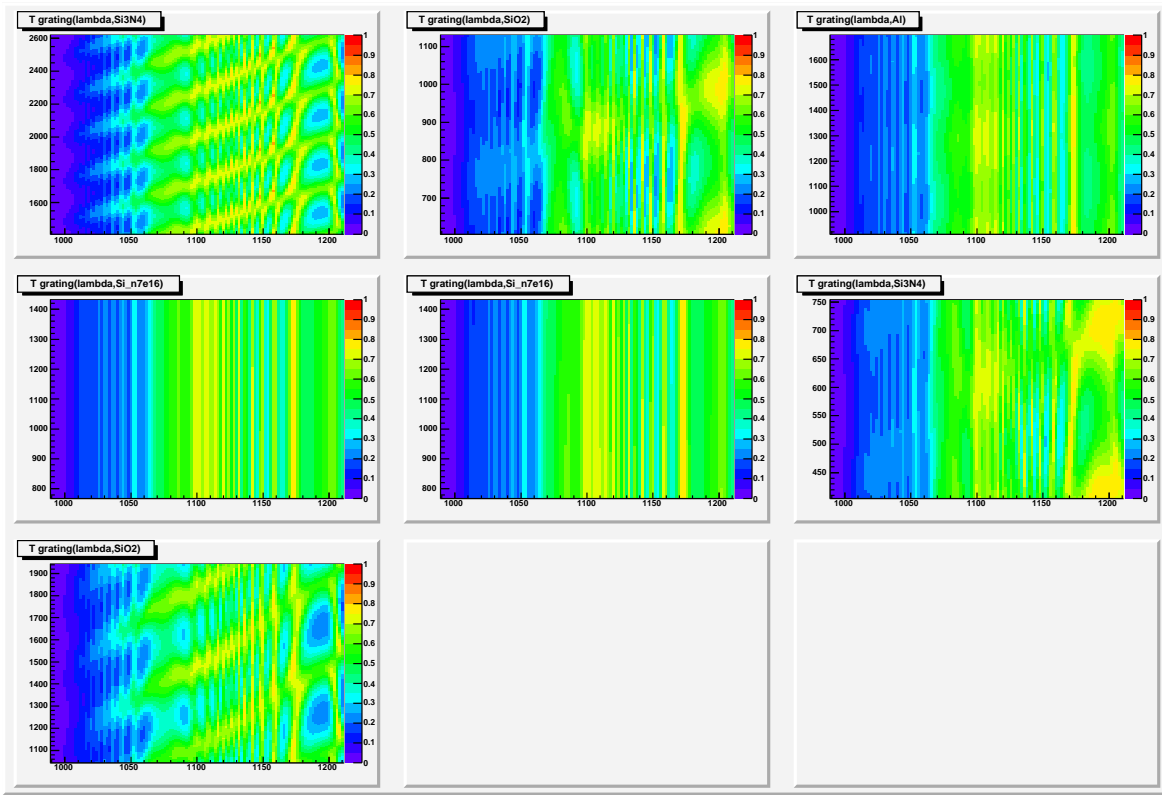


Figure 13: *Transmittance versus wavelength (horizontal axis) when one of the thicknesses of the materials is changed. Left to right, top to bottom, the changed layers are: Si_3N_4 , SiO_2 , Al, p implants, n implants, bottom Si_3N_4 and bottom SiO_2 layers. The remaining thicknesses are kept fixed as indicated in table 1*

6.1 Transparent or perfectly reflecting electrodes?

We can calculate now what is the advantage of having transparent electrodes in a design, instead of Al ones. The first action would be to substitute Al in the optimized design from last section by ITO. The result can be seen in Fig. 16. Since the refraction indexes of Al and ITO are different, the constructive interference conditions are not fulfilled anymore and the resulting transmittance with ITO is therefore lower than expected. We can then apply the optimization process described in last section to arrive to an optimum configuration using transparent electrodes, as that shown in Fig. 17. The absolute transmittance value with transparent electrodes is about 5% higher than with Al. If we try to use very thin layers of ITO (below 40 nm), the transmittance can reach up to 80%.

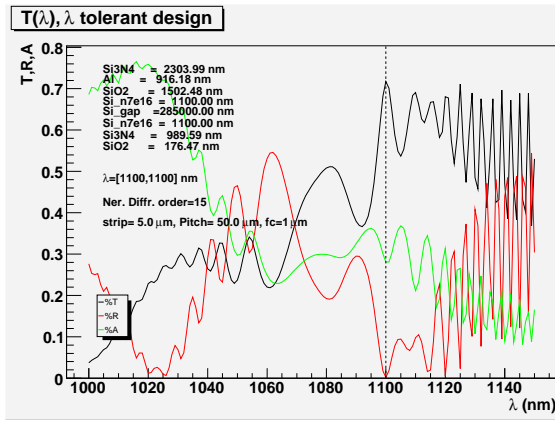


Figure 14: *Optical performance for the design shown in table 1*

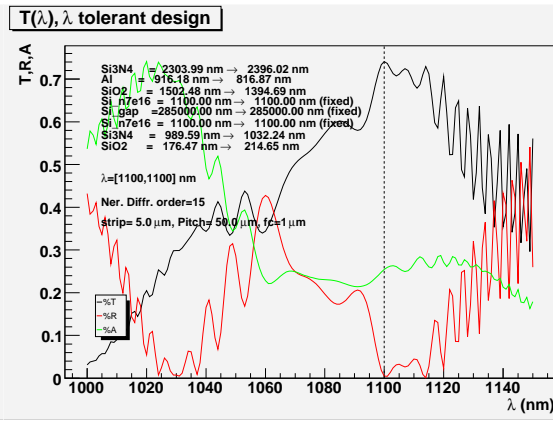


Figure 15: *Optimized performance at 1100 nm departing from the design shown in table 1 and Fig. 14.*

7 Conclusion

We have realistically simulated the balance of reflected, transmitted and absorbed energy in a microstrip silicon detector. Effects of diffraction in the strips are considered rigorously, changes of transmittance with doping and multiple interferences have also been taken into account.

The width of the strips and its pitch have been identified as key parameters limiting the amount of light traveling inside the detectors. The transmittance can be further increased under careful choice of the layer thicknesses.

Transparent electrodes have been studied as an option for Al electrodes. Indeed, the optical performance of the detectors is improved by 10% over the 70% achieved using Al. We believe ITO electrodes should be a solution worth trying as long as the technology deployment needed by such change is available in the house.

Acknowledgment

The authors would like to thank Dr. J.I. Larruquert and J.A. Méndez from Instituto de Física Aplicada-CSIC in Madrid, for enlightening guidance at the beginning of this work. We are indebt to Dr. L. Vanholme and Prof. Bienstmann from Photonics Research Group at the Department of Information Technology (INTEC) of Ghent University, for crosschecks of our simulation and specially for their help using CAMFR. We greatly acknowledge the free availability of RODIS and CAMFR and the quality of these 2

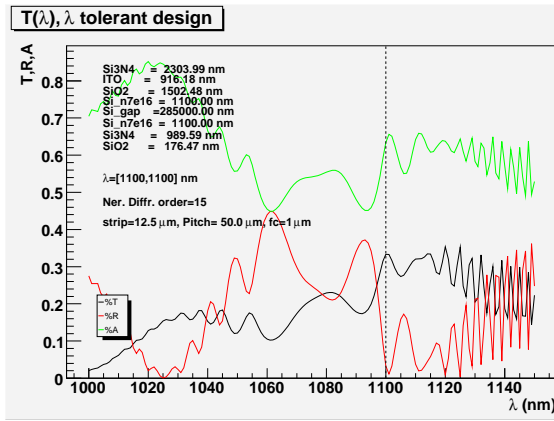


Figure 16: *Optical performance for the design shown in table 1 but with ITO instead of Al in the electrodes*

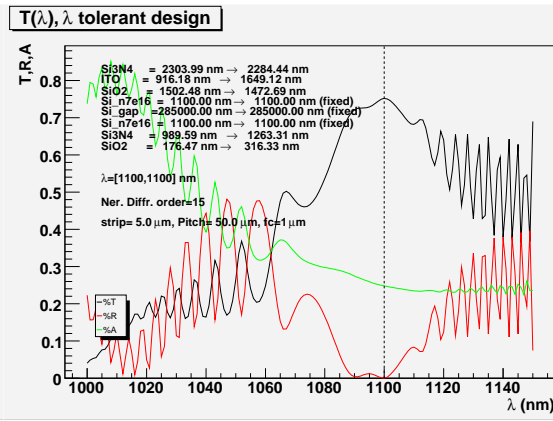


Figure 17: *Optimized performance at 1100 nm departing from the design shown in table 1 and Fig. 14. Using ITO for the electrodes.*

programs. We would also like to thank all members of the SiLC collaboration for helpful comments.

This work is supported by the Commission of the European Communities under the 6th Framework Programme "Structuring the European Research Area", contract number RII3-026126.

References

- [1] W. Wallraff, "TAS status", AMS Tracker Meeting, Montpellier, 22-23 June 2004.
- [2] The AMS collaboration, "The Alpha Magnetic Spectrometer (AMS) on the International Space Station, Part I, Results from the test flight on the Space Shuttle", Physics Reports, vol. 366/6 (Aug.2002), pp.331-404.
- [3] B. Wittmer et al., "The Laser Alignment System for the CMS Silicon Microstrip Tracker", Nucl. Instr. Meth. A581 (2007), p. 351
- [4] The CMS collaboration, "CMS Technical Design Report, Volume II: Physics Performance", J. Phys. G, Vol. 34, Num. 6, June 2007
- [5] J. Vandenhirtz, "Ein Infrarot Laser Positions-Kontroll-System für das AMS Experiment", PhD. Thesis, RWTH-Aachen, July 2001

- [6] W. Wallraff, AR sensor status, AMS TIM meeting, Houston, October 2002
- [7] L. Borrello et al., "Sensor design for the CMS Silicon Strip Tracker", CMS NOTE 2003/020
- [8] Hamamatsu Photonics Co., www.hamamatsu.com
- [9] SGS Thomsom Microelectronics, www.st.com
- [10] MSO Jena, Mikroschichtoptik GmbH Carl-Zeiss-Promenade 10 07745 Jena, Germany
- [11] R. Adolphi, "Construction and calibration of the Laser Alignment System for the CMS Tracker", PhD. thesis, RWTH-Aachen
- [12] E.D. Palik, "Handbook of Optical Constants of Solids", Academic Press; 1st edition (January 15, 1997)
- [13] M.J. Keevers, M.A. Green, "Absorption edge of silicon from solar cell spectral response measurements", Appl.Phys.Lett. 66 (2), 174-176, 9 January 1995
- [14] S.E. Aw et al, J. Phy. Condens. Matter 3 (1991) 8213-8223
- [15] R. Aaron Falk, "Near IR Absorption in Heavily Doped Silicon-An Empirical Approach", International Symposium for Testing and Failure Analysis, 2000
- [16] Max Born and E. Wolf, "Principles of Optics", Second Edition, Pergamon Press
- [17] H.A. Macleod, "Thin Film Optical Filters", Taylor & Francis; 3rd edition (January 1, 2001)
- [18] D. L. Windt, "IMD: Software for modeling the optical properties of multilayer films", Computers in Physics, July 1998, Vol. 12, Issue 4, pp. 360-370
- [19] R. Rivero, E. Romero, G. Gordillo, "Synthesis and Characterization of Highly Transparent and Conductive SnO₂:F and In₂O₃:Sn thin Films Deposited by Spray Pyrolysis", Brazilian Journal of Physics, vol. 36, no. 3B, Sept. 20006
- [20] D. Delbeke, "Design and fabrication of a highly efficient light-emitting diode: The grating-Assisted Resonant-Cavity Light-Emitting Diode", INTEC, University of Ghent, PhD thesis, 2002
- [21] Yu-Bin Chen, "Rigorous modeling of the radiative properties of micro/nanostructures and comparisons with measurements of fabricated gratings and slit arrays", PhD thesis, Georgia Institute of Technology, May 2007
- [22] P. Bientsmann, "Rigorous and efficient modelling of wavelength scale photonic components", INTEC, University of Ghent, PhD thesis, 2001

- [23] T. Clausnitzer et al., "An intelligible explanation of highly-efficient diffraction in deep dielectric rectangular transmission gratings", *Optics Express*, Vol. 13, Issue 26, pp. 10448-10456
- [24] B. Dhoedt, D. Delbeke, "RODIS: Rigorous Optical Diffraction Software",
<http://www.photonics.intec.ugent.be/research/facilities/design/rodis/>
- [25] P. Bienstmann, L. Vanholme, "CAMFR: Cavity Modelling Framework",
<http://camfr.sourceforge.net/>
- [26] L. Vanholme et al., "Python in Nanophotonics Research, Computing in Science & Engineering", 9(3), p.46-47 (2007)
- [27] M. Fernández et al., "IR transmittance optimization for a CMS silicon microstrip sensor", in preparation.